Local Conformation of Rabbit Skeletal Myosin Rod Filaments Probed by Intrinsic Tryptophan Fluorescence†

Yoke-chen Chang and Richard D. Ludescher*

Department of Food Science, Rutgers University, and New Jersey Agricultural Experiment Station, Cook College, New Brunswick, New Jersey 08903-0231

Received August 9, 1993; Revised Manuscript Received November 22, 1993®

ABSTRACT: Rabbit skeletal myosin rod contains two tryptophan residues per chain (four per coiled-coil) that are located about 50 and 175 Å from the N-terminus of the light meromyosin (LMM) region of rod. We have characterized the local polarity, excited-state photophysics, solvent accessibility, and rotational dynamics of these tryptophans in myosin rod filaments at 125 mM KCl using steady-state and time-resolved fluorescence techniques. The fluorescence decays were described using a complex bimodal distribution with a discrete long-lifetime component of 5.44 ns (amplitude of 0.51) and a Gaussian distribution of short lifetimes with mean of 0.105 ns and width of 2.15 ns (amplitude 0.49). The discrete long-lifetime species was efficiently quenched by the neutral quencher acrylamide with a bimolecular collision constant (k_q) of 0.85×10^9 M^{-1} s^{-1}. The emission spectrum, lifetime distribution, and quenching behavior of the tryptophans in myosin rod monomers (at 0.5 M KCl) were quite similar. Time-resolved anisotropy decays of the rod monomers and filaments exhibited nearly identical double-exponential decays to a constant. Each had a fast, subnanosecond component (amplitude 0.07), probably corresponding to fast wobble of the tryptophans on the coiled-coil surface, a slower, ≈6-ns component (amplitude ≈0.04), corresponding to an unidentified internal, segmental mode of motion of the coiled-coil, and a constant (r_∞) of 0.15. This study demonstrated that there were no significant differences in the chemical or physical environment of the rod tryptophans in the two aggregation states of the protein, indicating that the region of LMM containing these tryptophans was not tightly aggregated into the body of the thick filament. This work suggests that the myosin crossbridge may be nearly 300 Å longer than previous models have postulated.

Vertebrate striated muscles convert the chemical energy of ATP hydrolysis into the microscopic vectorial movement of large filament complexes (Cooke, 1986). This energy transduction process (Eisenberg & Hill, 1985) takes place within the sarcomere, an elaborate, subcellular complex of parallel and overlapping thick (myosin-containing) and thin (actin-containing) filaments (Bagshaw, 1982). The overall sarcomere length decreases during muscle contraction through a change in the extent of overlap among the interdigitated thick and thin filaments (Huxley & Niedergerke, 1954; Huxley & Hanson, 1954); this is generally referred to as the sliding filament model. The relative sliding of the thick and thin filaments is driven by a cycle of actin binding and release by projections from the thick filament called crossbridges (Tregear & Marston, 1979). The energy for the cyclic interaction between the crossbridge and actin is provided by the hydrolysis of MgATP (Kodama, 1985).

Vertebrate skeletal myosin is a large (≈520 kDa) hexameric protein composed of two identical heavy and four light chains (Harrington & Rodgers, 1984). The N-terminal portions of the heavy chains (about 850 residues) fold into the 2 globular heads of myosin (Warrick & Spudich, 1987; Rayment et al., 1993); the C-terminal portions (about 1000 residues) of 2 identical chains fold into a nearly continuous region of α-helical coiled-coil structure, the myosin tail (Lowey & Cohen, 1962). Two light chains associate with each globular head along a long helix that forms the C-terminus of the head (Rayment et al., 1993). Myosin can be readily cleaved at the head/tail junction to produce free globular heads (subfragment 1, S1)[1] plus the tail (myosin rod) (Lowey et al., 1969; Margossian & Lowey, 1982). There is a region within the tail about one-third of the distance to the C-terminus that is sensitive to proteolysis (Lowey & Cohen, 1962; Weeds & Taylor, 1975); this so-called hinge region is also believed to be a site of enhanced flexibility (Huxley, 1969; Harvey & Cheung, 1982). Cleavage at the hinge produces an N-terminal tail fragment (S2) and light meromyosin (LMM) (Margossian & Lowey, 1982).

In high-salt buffer (≥300 mM), the myosin molecule is primarily monomeric (that is, exists as a single hexamer). Under low-salt conditions, the molecule aggregates into thick filaments containing several hundred myosin molecules (Pepe, 1983). The myosin filaments in vertebrate skeletal muscle are bipolar (Huxley, 1963); myosin monomers aggregate in a tail-to-tail fashion in a central bare zone of the filament and aggregate outward from this bare zone in a head-to-tail fashion. The packing arrangement in the body of skeletal muscle myosin and LMM filaments has been studied by X-ray diffraction (Huxley & Brown, 1967; Katsura & Noda, 1973a,b). In both types of filaments, the coiled-coil LMM region is thought to aggregate into the body of the filaments with the coiled-coil

† Publication No. D-10115-3-93 of the New Jersey Agricultural Experiment Station. This work was supported in part by the State of New Jersey, by a Grant-in-Aid of Research from Sigma Xi, the Scientific Research Society (to Y.C.), and by NIH Grant RR01348 to the Regional Laser and Biotechnology Laboratory.

* Address correspondence to this author at the Department of Food Science, Rutgers University.

® Abstract published in *Advance ACS Abstracts,* February 1, 1994.

[1] Abbreviations: EDTA, ethylenediaminetetraacetic acid; FWHM, full width at half-maximum; MB, myosin buffer; KDP, potassium dihydrogen phosphate; LMM, light meromyosin; MB, myosin buffer; MOPS, 4-morpholinepropanesulfonic acid; NATA, *N*-acetyltryptophanamide; NdYAG, neodymium yttrium aluminum garnet; SDS, sodium dodecyl sulfate; S1, subfragment 1; S2, subfragment 2.

0006-2960/94/0433-2313$04.50/0

axes parallel to the long axis of the filaments (Pepe, 1982). The aggregation is mediated by electrostatic interactions among the surface residues of the coiled-coil although the exact details of the aggregation mechanism remain unknown. The crossbridges that project from the thick filaments are composed of the two globular heads plus some part of the coiled-coil rod (Pepe, 1967; Huxley & Brown, 1967; Huxley, 1969). Since the hinge region is thought to facilitate the extension of the crossbridge away from the filament surface, most models postulate that the body of the thick filament consists of a bundle of LMM regions while the crossbridge consists of the S2 region plus the two globular heads.

Myosin rod contains 2 tryptophans per heavy chain (Maeda et al., 1987; King & Lehrer, 1989) located at nonpolar "d" sites in the heptad repeat that forms the basis for hydrophobic association of the α-helixes into a coiled-coil (McLachlan & Karn, 1982); these tryptophans are located in the LMM region 33 and 118 residues (that is, about 50 and 175 Å) away from the arginine that denotes the C-terminus of the putative hinge region (Lu & Wong, 1985; Maeda et al., 1987). The location of these residues is indicated schematically in Figure 1. We have studied the fluorescence properties of these residues in the myosin rod at high salt (under conditions where the rod is monomeric) in an effort to characterize the local structure and environment of the coiled-coil region of myosin (Chang, 1993; Chang & Ludescher, 1992, 1993, 1994). We report herein a similar study of the tryptophans in filaments formed by dilution of myosin rod from high- into low-salt buffer. This study, which involved steady-state and time-resolved measurements of fluorescence intensity, quenching, and polarization, indicated that the local environment of the tryptophans in rod filaments was essentially identical to that found in rod monomers. Since the tryptophans are located in a region of the rod that is thought to aggregate into the body of the thick filament (Huxley & Brown, 1967; Pepe, 1967; Huxley, 1969), this study suggests that the crossbridge may be much longer than previous models have indicated.

MATERIALS AND METHODS

Protein Preparations. Myosin was extracted from the skeletal muscle of New Zealand white rabbits. Myofibrils were prepared from the minced leg and back muscle (Thomas et al., 1980), and myosin was purified from myofibrils as described in Eads et al. (1984). The purified myosin was stored at −20 °C in myosin buffer (MB, see below) containing 50% glycerol (v/v) as an antifreeze. The myosin rod was prepared from myosin by digestion with α-chymotrypsin (Sigma Chemical Co., St. Louis, MO) at room temperature at low ionic strength in the absence of Mg^{2+} (0.12 M KCl, 20 mM MOPS, and 1 mM EDTA, pH 7.0) using published methods (Weeds & Taylor, 1975) and purified from S1 and undigested myosin by ethanol precipitation (Harrington & Burke, 1972). The purity of rod samples was checked by SDS–polyacrylamide gel electrophoresis (Eads et al., 1984). The rod preparations used to collect the data herein showed one dominant band in 10% polyacrylamide gels. Densitometry of stained gels indicated that the protein was ≥95% rod with the remainder smaller fragments. The purified myosin rod was stored at −20 °C in MB plus 50% glycerol (v/v). Filaments were formed by diluting rod in MB (containing 0.5 M KCl) with sufficient MB without KCl to generate a filament solution with 0.125 M KCl (low-salt MB, see below). The composition of these buffers is as follows: MB, 0.5 M KCl, 0.5 mM EDTA, 0.5 mM dithiothreitol, and 20 mM MOPS, pH 7.0; low-salt MB, 0.125 M KCl, 0.5 mM EDTA, 0.5 mM dithiothreitol, and 20 mM MOPS, pH 7.0.

The fraction of rod aggregated into filaments was evaluated by a comparison of the soluble protein concentration after ultracentrifugation of a filament solution (in low-salt MB) with that of a monomer solution (in MB). Myosin rod was dialyzed overnight against MB buffer and diluted into either MB or low-salt MB to a final protein concentration of 0.2 mg/mL. The two solutions were centrifuged (45 000 rpm for 60 min in a 50Ti rotor), and the fluorescence emission intensity of the supernatants of the two solutions was measured under identical instrumental conditions (excitation at 300 nm and emission at 350–360 nm using the filter combination described below). At these protein concentrations, where the optical density of the rod monomer solution was 0.04, the fluorescence intensity is linear with protein concentration (Lakowicz, 1983). By this fluorescence criterion, 91% of the rod sedimented under our experimental conditions and was thus aggregated into filaments. Since the protein concentration used in this assay (0.2 mg/mL) was lower than that typically used for our fluorescence measurements, this was an underestimate of the fraction of rod aggregated into filaments in our fluorescence measurements.

Steady-State Spectroscopic Measurements. All steady-state fluorescence intensity measurements were made on a SPEX F1T11 spectrofluorometer equipped with a temperature-controlled sample holder. An ultraviolet interference filter (catalog no. 59610; Oriel Co., Stratford, CT) with a center wavelength at 300 nm (bandwidth 10 nm) was placed in the sample compartment after the excitation monochromator, and a long-pass 324-nm cuton filter (catalog no. 59458, Oriel Co.) was placed in the sample compartment before the emission monochromator; these filters eliminated any scattering artifacts from the slightly turbid filament solutions. Emission spectra were typically collected with 1.9-nm band-pass resolution using excitation at 300 nm.

Steady-State Quenching Measurements. Aliquots from a freshly prepared 2 M stock solution of acrylamide (electrophoresis grade) were added as a quencher to a 1.7-mL sample of myosin rod monomers (0.2 mg/mL) or NATA (10 μM) in MB or myosin rod filaments (0.2 mg/mL) in low-salt MB at 20 °C. Quenching measurements were performed using excitation at 300 nm (0.38-nm band-pass) and emission at 360 nm (30-nm band-pass). All fluorescence intensity measurements were corrected for dilution effects, and corrections were made for acrylamide absorption at 300 nm using an extinction coefficient for acrylamide at 300 nm of 0.15 M^{-1} cm^{-1} (maximum adjustment was 5% at 1.2 M acrylamide). These data were plotted as the ratio of the fluorescence intensity in the absence (F_0) to the intensity in the presence (F) of quencher versus the quencher concentration. The quenching curves were fit to the modified Stern–Volmer equation (eq 1) (Eftink, 1991) In eq 1, [Q] is the concentration of quencher,

$$F_0/F = (1 + K_{sv}[Q]) \exp(V[Q]) \quad (1)$$

K_{sv} is the Stern–Volmer quenching constant ($=k_q\tau_0$, where k_q is the bimolecular quenching constant and τ_0 is the lifetime in the absence of quencher), and the exponential term includes the possibility of static quenching with a quenching constant V (Eftink & Ghiron, 1976).

In those cases where the Stern–Volmer plots showed downward curvature, the quenching results were analyzed as the ratio F/F_0 versus quencher concentration using the expression (Eftink, 1991):

$$F/F_0 = \sum_{i=1}^{n} f_i/(1 + K_{sv,i}[Q]) \quad (2)$$

where f_i is the fractional fluorescence intensity (fraction of the total fluorescence intensity due to component i, see eq 4 below) and $K_{sv,i}$ is the Stern–Volmer quenching constant for component i. Data for myosin rod monomers and rod filaments were fit to this equation using least-squares fitting procedures (as above). Equation 2 was also modified to account for the possibility of static quenching:

$$F/F_0 = \sum_{i=1}^{n} f_i/(1 + K_{sv,i}[Q]) \exp(V[Q]) \quad (3)$$

Time-Resolved Measurements. Fluorescence total intensity (lifetime) decay measurements were performed on the time-correlated single photon counting fluorometer at the Regional Laser and Biotechnology Laboratory (RLBL), Department of Chemistry, University of Pennsylvania. This instrument uses as a light source the doubled output of a Coherent Antares mode-locked NdYAG laser pumping a dye laser. The red dye laser output from rhodamine 6G, cavity-dumped at 4 MHz, was doubled in a KDP crystal to an excitation wavelength in the range from 280 to 300 nm. Instrument response functions, generated by scattering excitation light from a solution of coffee creamer, and total intensity decays from myosin rod emission were collected using magic-angle polarization following vertically polarized excitation. This instrument uses a Hamamatsu microchannel plate detector; typical instrument response curves had a FWHM of about 25 ps.

The lifetime decays of myosin rod filaments were collected as a function of the concentration of the quencher acrylamide at constant ionic strength by using excitation at 290 nm and emission at 350 nm (band-pass 20 nm). Previous steady-state and time-resolved studies have indicated that there was no tyrosine emission with excitation at this wavelength (Chang, 1993; Chang & Ludescher, 1994). The decays for each quenching set (that is, for each set of decays at different quencher concentrations) were analyzed simultaneously using global fitting routines on the program Globals Unlimited (University of Illinois) that was developed by Beechem and colleagues (Beechem & Gratton, 1988; Beechem et al., 1991). Global fits were done using different possible models for the decay behavior that involved either distributions of lifetimes or discrete lifetimes. The goodness-of-fit was evaluated by examination of the value of the global χ^2 and plots of the modified residuals and autocorrelation functions for the individual data sets. A fit was considered appropriate when the modified residuals and autocorrelation functions showed random deviations about zero and the global χ^2 value was less than 3 (Beechem et al., 1991).

The lifetime components (τ) were plotted as τ_0/τ vs [Q], where τ_0 is the lifetime in the absence of quencher and τ is the lifetime in the presence of quencher. These plots were analyzed using the Stern–Volmer quenching formalism (eq 1) but without the static quenching term (that is, V was set equal to 0 for the fit). The value of τ_0 was also used to calculate the collisional rate constant (k_q) from the Stern–Volmer quenching constant (K_{sv}) in both steady-state and time-resolved quenching studies.

The fractional fluorescence intensity (f_i in eq 2 and 3) is related to the normalized amplitude a_i (the mole fraction) of each lifetime component τ_i determined from lifetime decays:

$$f_i = a_i\tau_i/\sum a_i\tau_i \quad (4)$$

Time-Resolved Anisotropy Decays. The time-resolved anisotropy measurements were done using methods similar to the lifetime measurements (see above) except that the emission was collected through polarizers oriented alternately parallel and perpendicular to the vertically polarized excitation light; this procedure generated parallel [$I_\parallel(t)$] and perpendicular [$I_\perp(t)$] decay transients. The anisotropy decay was calculated as

$$r(t) = [I_\parallel(t) - I_\perp(t)]/[I_\parallel(t) + 2I_\perp(t)] \quad (5)$$

The sensitivities of the detection system for vertically and horizontally polarized light, measured in independent experiments, was unity for the laser system at the RLBL used for this study. Anisotropy decays were collected with excitation at 300 nm and emission at 360 nm (20-nm band-pass).

The calculated anisotropy decays were analyzed directly as a sum of exponentials plus a constant (Belford et al., 1972) using the nonlinear least-squares iterative fitting program NFIT. The function used for fitting was

$$r(t) = \sum r_i \exp(-t/\phi_i) + r_\infty \quad (6)$$

where the sum was over either one- or two-exponential terms. The ϕ_i terms are the rotational correlation times for the rotational motion of the chromophore, and the r_i terms are complex, model-dependent amplitudes for the rotational motion (Steiner, 1991). The goodness-of-fit of a function was determined by examination of the residuals of the fit (calculated fit – data) and evaluation of χ^2. The zero time point for anisotropy fits was chosen as the peak of the lamp function.

Attempts to fit the individual vertical and horizontal polarization transients to a product of the total intensity decay times a function of the anisotropy decay using standard deconvolution techniques (Barkley et al., 1981; Steiner, 1991) were unsuccessful. We attribute this failure to the complexity of a deconvolution analysis in which the total intensity decay was described by a bimodal distribution involving a discrete lifetime and a Gaussian distribution of lifetimes and the anisotropy decay was described by a single- or double-exponential decay to a constant. Since the instrument response function used in these experiments had a full width at half-maximum of 25 ps (see Figure 7), and thus only the initial data points of the anisotropy decays (≈100 ps) were subject to convolution artifacts (Papenhuijzen & Visser, 1983), a direct analysis of the calculated anisotropy decay provided a reasonable and accurate method of analysis for all but data at very short times (≤100 ps).

The rotational correlation time for a globular protein treated as a rotating sphere is given by the Einstein relation:

$$\phi = V\eta/RT \quad (7)$$

where V is the hydrated molar volume, η is the solution viscosity (equal to 0.01 P for water at 20 °C), R is the gas constant, and T is the absolute temperature. The equivalent molecular weight for the rotating sphere can be estimated by dividing the molar volume by 1.0 cm^3/g, the partial specific volume of a typical protein hydrated to about 0.25–0.3 g of water/g of protein (Cantor & Schimmel, 1980). The correlation time for rotation about the long axis of the rod was estimated as two-thirds of the correlation time expected for a sphere with molecular mass of 200 kDa (Cantor & Schimmel, 1980).

RESULTS AND DISCUSSION

Steady-State Fluorescence Intensity. Rabbit skeletal myosin rod contains two tryptophans per chain located in LMM near the hinge region that forms the junction between S2 and

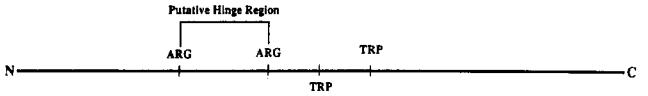

FIGURE 1: Schematic diagram of the structure of rabbit skeletal myosin rod showing the location of the two tryptophans (Trp). The hinge region that separates short S2 (sS2) from the light meromyosin (LMM) region is defined by the location of two proteolytically sensitive arginine (Arg) residues.

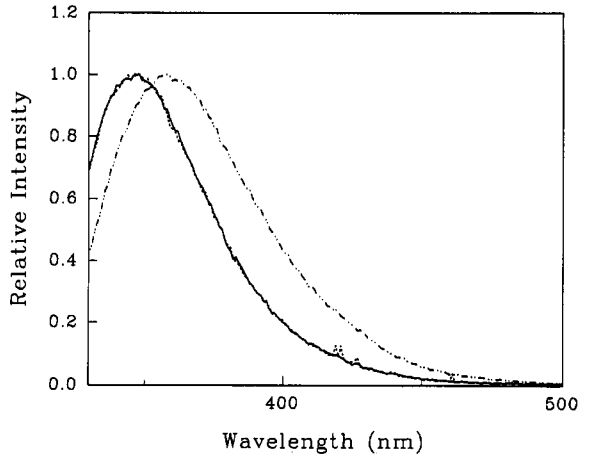

FIGURE 2: Normalized emission spectra of L-tryptophan in MB (– •• –), myosin rod monomers in MB (•••), and myosin rod filaments in low-salt MB (—); spectra collected at 20 °C.

LMM (King & Lehrer, 1989; Maeda et al., 1987). These tryptophans are thus excellent intrinsic probes that can be used to characterize the detailed structure and dynamics of the N-terminal region of LMM (Figure 1). Since over 90% of the rod was aggregated into filaments in low-salt buffer under the conditions of our experiments (see Materials and Methods), we were able to make a detailed comparison of the influence of filament formation on the fluorescence properties of these tryptophans. Myosin rod monomers and L-tryptophan were studied as controls.

The steady-state tryptophan emission spectra of myosin rod filaments, myosin rod monomers, and L-tryptophan were collected at 20 °C using a 300-nm interference filter at the excitation and a 324-nm UV cuton filter at the emission in order to prevent artifacts due to scattering by the filaments. These spectra are shown in Figure 2. The emission maxima of these spectra were at 348, and 347, and 358 nm for myosin rod filaments, rod monomers, and NATA, respectively. The emission maximum of rod monomers collected using these filters was red-shifted about 7 nm compared with the maximum of monomers collected without filters (Chang, 1993; Chang & Ludescher, 1994); we attribute this shift to a spectral distortion caused by the emission filter. In spite of this, the emission maximum of rod monomers showed a blue-shift of about 10 nm compared to that of L-tryptophan. The emission spectrum of rod filaments was indistinguishable from that of monomers (Figure 2) and also showed a blue-shift of about 10 nm compared to the emission of L-tryptophan. There was thus no indication of a wavelength shift of the tryptophan emission in rod monomers upon aggregation into filaments, suggesting little or no change in the polarity of the local environment of the tryptophans (Demchenko, 1986) upon aggregation into filaments. The tryptophans in myosin rod filaments thus appeared to be in a partially solvent-exposed environment that was similar to the average environment of tryptophans in myosin rod monomers (Chang, 1993; Chang & Ludescher, 1994).

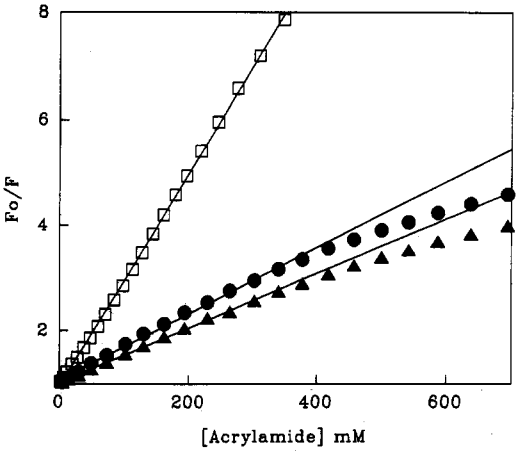

FIGURE 3: Stern–Volmer plots of the ratio of the tryptophan fluorescence intensity in the absence (F_0) and presence (F) of the quencher acrylamide. The data are NATA in MB (□), myosin rod monomers in MB (●), and myosin rod filaments in low-salt MB (▲). Data collected at 20 °C.

Steady-State Acrylamide Quenching. Fluorescence quenching of NATA, filaments, and monomers by acrylamide was collected using the filter system described above; typical Stern–Volmer plots are shown in Figure 3. The plots were approximately linear for NATA; analysis using a single-component dynamic–static model (eq 3, Materials and Methods) gave a Stern–Volmer (K_{sv}) quenching constant of 17.5 M^{-1} and a static quenching constant (V) of 0.47 M^{-1} (Table 1). These values are similar to those reported by other researchers (Eftink, 1991).

The Stern–Volmer plots showed downard curvature, however, for both monomers and filaments, indicating that there were at least two populations of tryptophans with different K_{sv} values (Lehrer, 1971; Eftink, 1991). The K_{sv} values for monomers from a two-component dynamic analysis (eq 2) were 8.38 ± 0.24 and <0.04 M^{-1} with fractional amplitudes of 0.93 and 0.07, respectively (Table 1); analysis using a two-component dynamic–static model (eq 3) gave identical results with a static quenching constant of zero. These results for monomer quenching obtained using filters were identical to previous data collected without filters (Chang & Ludescher, 1993), indicating that the use of filters did not compromise the experimental quenching results.

The acrylamide quenching data for filaments were also analyzed using two-component dynamic (eq 2) and dynamic–static (eq 3) quenching models; the K_{sv} values from these analyses were identical (with $V = 0$). A representative data curve fit using a two-component dynamic model is plotted as the ratio F/F_0 in Figure 4. The Stern–Volmer constants for filament quenching, 6.20 ± 0.07 and <0.04 M^{-1} with fractional amplitudes of 0.93 and 0.07, respectively (Table 1), were quite similar to the values seen in rod monomers (Table 1). The slight decrease in K_{sv} for the major quenching component in filaments may reflect the influence of the larger size, and thus smaller diffusion coefficient, of the filament (Noyes, 1961).

Time-Resolved Fluorescence Intensity. The intensity decays of filaments in the absence of quencher were well fit using a bimodal model with a discrete long lifetime and a Gaussian distribution of short lifetimes; χ^2 values for this analysis were in the range from 1.04 to 1.10, and residuals and autocorrelation plots were flat and random for all data sets. The fit lifetime distributions from the bimodal discrete/Gaussian model are plotted in Figure 5. The discrete long lifetime was 5.44 ns with a normalized amplitude of 0.51, and the Gaussian distribution of short lifetimes was centered

Table 1: Stern–Volmer (K_{sv}) and Bimolecular Collision (k_q) Constant for Acrylamide Quenching of Tryptophan Fluorescence in NATA and in Myosin Rod Monomers and Filaments at 20 °C

	Stern–Volmer constant			k_q ($\times 10^9$ M^{-1} s^{-1})	
	intensity[a]		lifetime[b]		
	$K_{sv,i}$ (M^{-1})	V (M^{-1})	K_{sv} (M^{-1})	intensity	lifetime
NATA	17.5 ± 0.12	0.47		5.83 ± 0.04[c]	
monomer	8.38 ± 0.24		6.18 ± 0.35	1.55 ± 0.44[d]	1.14 ± 0.065[d]
	<0.4		≤0.5	<0.4[e]	≤0.6[e]
filament	6.20 ± 0.07		4.63 ± 0.15	1.14 ± 0.013[f]	0.85 ± 0.028[f]
	<0.04		≤0.6	<0.4[g]	[h]

[a] Stern–Volmer quenching constants from analysis of steady-state quenching data using one-component analysis for NATA (eq 1, Materials and Methods) and two-component analysis for myosin rod (eq 2). The errors are from the mean of duplicate data sets. [b] Stern–Volmer quenching constants from analysis of time-resolved quenching data from duplicate data sets. The data for rod monomers are from Chang and Ludescher (1993). [c] Calculated using τ = 3.0 ns (Szabo & Rayner, 1980). [d] Calculated using the long lifetime, τ = 5.40 ns (Chang & Ludescher, 1993). The errors were calculated by propagation of measured errors in K_{sv} and τ. [e] Calculated using the mean of the short-lifetime distribution, $\bar{\tau}$ = 0.90 ns (Chang & Ludescher, 1993). [f] Calculated using the long lifetime, τ = 5.44 ns. The errors were calculated by propagation of measured errors in K_{sv} and τ. [g] Calculated using the mean of the short-lifetime Gaussian distribution, $\bar{\tau}$ = 0.105 ns. [h] Calculation leads to a physically unreasonable result for k_q (≤5 × 10^9 M^{-1} s^{-1}).

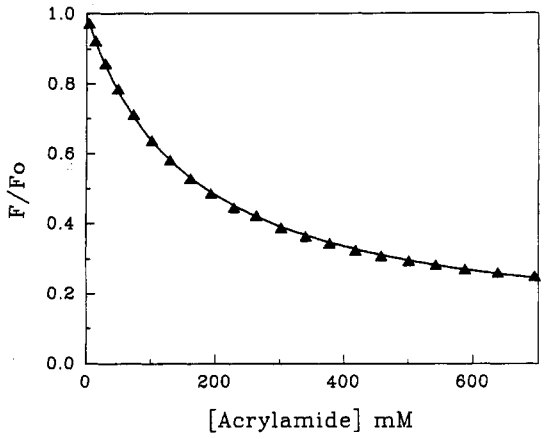

FIGURE 4: Quenching of tryptophan fluorescence in myosin rod filaments at 20 °C in low-salt MB by acrylamide. The data are plotted as the ratio of the fluorescence intensity in the presence (F) to the intensity in the absence (F_0) of quencher. The smooth curve is a two-component fit to the data using a dynamic quenching model (eq 2, Materials and Methods). Details in text and in Table 1.

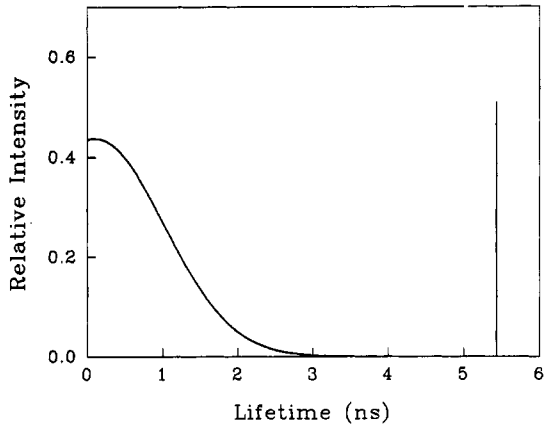

FIGURE 5: Bimodal discrete/Gaussian distribution of lifetimes used to describe the intensity decay of tryptophan fluorescence in myosin rod filaments in low-salt MB at 20 °C. The long lifetime was 5.44 ns (normalized amplitude of 0.51), and the Gaussian distribution had a mean of 0.105 ns with FWHM of 2.15 ns (normalized amplitude of 0.49). See text for additional details.

around 0.105 ns (FWHM of 2.15 ns) with a normalized amplitude of 0.49.

The values for this bimodal lifetime distribution in filaments were quite similar to those found previously for rod monomers (Chang & Ludescher, 1994). The discrete long lifetimes were nearly identical with values of 5.44 ns in filaments and 5.40 ns in monomers. The short-lifetime distribution, however, had a smaller mean in filaments, 0.105 ns, than in monomers, 0.91 ns, while its amplitude was larger in filaments, 0.49, than it was in monomers, 0.21. A comparison of these photophysical properties suggests that the local chemical environment of the four tryptophans in the rod was also similar in the two aggregation states. The changes in the short-lifetime distribution and amplitude probably reflected subtle changes in the local packing of protein side chains about the indole rings rather than gross changes in the chemical environments of the tryptophan side chains.

Time-Resolved Acrylamide Quenching. Intensity decays of the rod filament fluorescence collected as a function of acrylamide concentration over the range from 0 to 200 mM acrylamide were well fit using a model in which a Gaussian distribution of short lifetimes was linked (constrained to the same values) across all data sets, while a discrete, long lifetime and the amplitudes of all components were allowed to vary across all data sets. The modified residuals from this analysis for individual intensity decays quenched by various concentrations of acrylamide are plotted in Figure 6; the low χ^2 values for these analyses, in the range from 1.01 to 1.22, and the flat and random residuals plots demonstrated that this model was an excellent description of the data.

The global analyses of acrylamide quenching indicated that only the discrete, long-lifetime component in rod filaments was efficiently quenched by acrylamide; an identical result was seen in acrylamide quenching of rod monomers (Chang & Ludescher, 1994). As the concentration of acrylamide increased from 0 to 200 mM, the discrete long lifetime in the filament decreased from 5.44 to 2.98 ns while the Gaussian distribution of short lifetimes remained unchanged. A Stern–Volmer analysis of the quenching of the long-lifetime component is plotted in Figure 7. This plot is linear (correlation coefficient of 0.997) with a slope of 4.63 M^{-1} over the range of acrylamide concentration from 0 to 125 mM. The higher values of the data points for acrylamide concentrations above 120 mM may be due to inherent difficulties in the resolution of the quenched long-lifetime component from the short-lifetime distribution of components; as the long-lifetime component was quenched, it began to overlap more and more closely the short-lifetime distribution (Figure 5). The normalized amplitudes (mole fractions) of the discrete long-lifetime component remained constant at about 0.51 over the range of acrylamide concentration from 0 to 80 mM but decreased at higher acrylamide concentrations. Similar behavior was seen in the monomer quenching study (Chang & Ludescher, 1993).

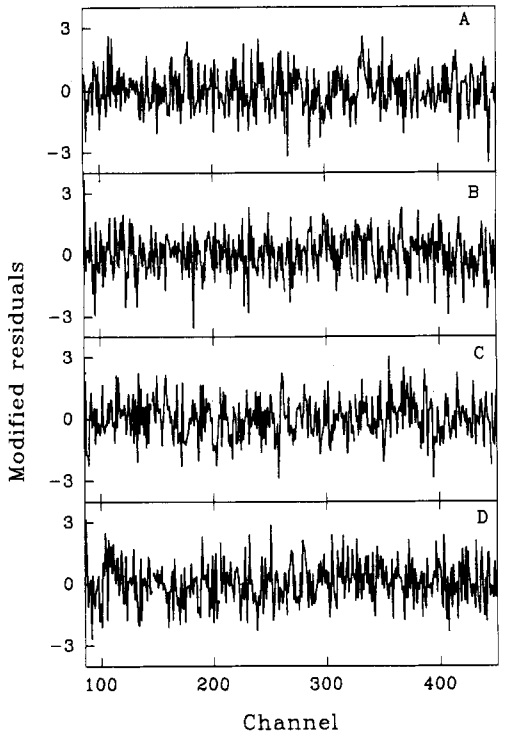

FIGURE 6: Modified residuals for global analysis of acrylamide quenching of the fluorescence from rod filaments in low-salt MB at 20 °C using a bimodal discrete/Gaussian distribution model. The Gaussian distribution of short lifetimes was linked across all data sets (mean lifetime of 0.105 ns, FWHM of 2.15 ns), and the discrete, long-lifetime component and the amplitudes of both components were varied across all data sets. The residuals plots are for fits to decays in the presence of acrylamide concentrations of 0 (A), 40 (B), 100 (C), and 120 mM (D).

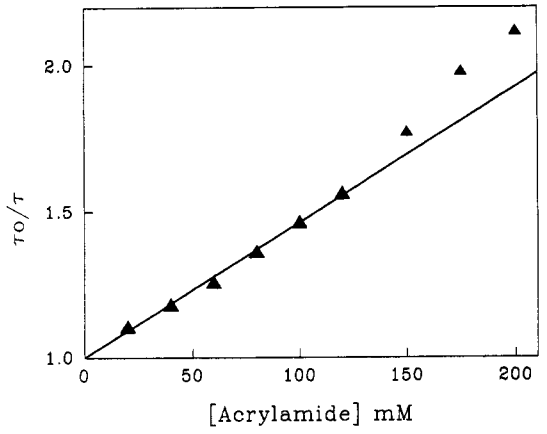

FIGURE 7: Stern–Volmer plot of the ratio of the tryptophan long lifetime in the absence (τ_0) and presence (τ) of quencher for acrylamide quenching of rod filaments in low-salt MB at 20 °C. The line is a linear least-squares fit to the data over the range 0–120 mM acrylamide. Details in text and in Table 1.

The global analysis thus indicated that the long-lifetime component in filaments was quenched with a K_{sv} of 4.63 ± 0.15 M^{-1} (Table 1). Assuming that the global analysis cannot detect a 10% decrease in the mean of the short-lifetime distribution, the K_{sv} for quenching the distributed component was estimated to be less than 0.6 M^{-1} (Table 1). These data thus suggest that the two components seen in the steady-state quenching data correspond to efficient quenching of the discrete long-lifetime component and inefficient quenching of the Gaussian distribution of short-lifetime components.

Bimolecular Quenching Constants. The collision constants for dynamic quenching of filament tryptophan fluorescence

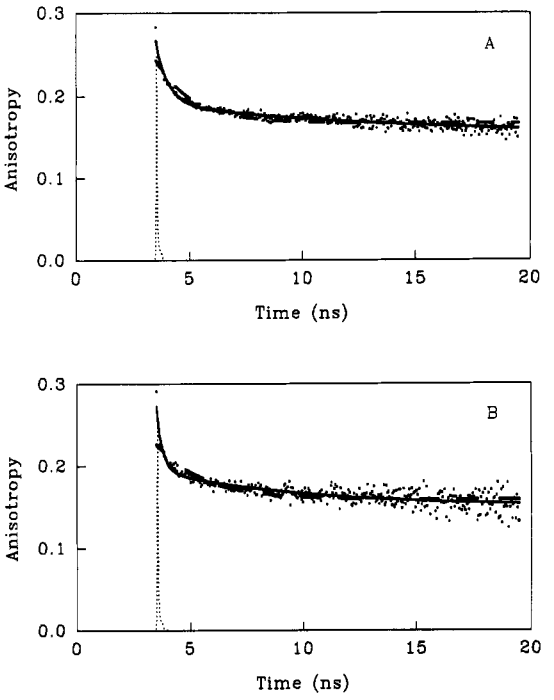

FIGURE 8: Anisotropy decays of the tryptophan fluorescence from myosin rod monomers in MB (A) and myosin filaments in low-salt MB (B). The anisotropy decays were calculated directly from the parallel and perpendicular decay transients; the smooth curves through the data correspond to single (—) and double (– –) exponential decays to a constant (eq 6, Materials and Methods).

by acrylamide, calculated from the quenching constants determined in steady-state and time-resolved experiments, are summarized in Table 1. The bimolecular rate constant for collision of acrylamide with the discrete long-lifetime tryptophan species in filaments was 0.85×10^9 M^{-1} s^{-1}; this value is only slightly smaller than 1.14×10^9 M^{-1} s^{-1}, the rate constant for acrylamide quenching of the long-lifetime component in monomers (Chang & Ludescher, 1993). Since k_q is the rate constant for diffusional collisions of the quencher with the tryptophans in the protein, the difference certainly reflects the effect of the smaller diffusion coefficient of the much larger filament complex (Noyes, 1961).

The ratio of the collisional rate constant (k_q) for a particular fluorescent species to that of NATA can provide a measure of the accessibility of that species to the quencher (Johnson & Yguerabide, 1985). This ratio for the long-lifetime component in filaments was 0.18. For a complex the size of rod filaments, the k_q ratio would be about 0.38 for a fully solvent-accessible, surface tryptophan (Johnson & Yguerabide, 1985); comparison of these two ratios allowed an estimate of the fractional accessibility to acrylamide of the long-lifetime species in filaments. This fractional accessibility, about 20–23%, was nearly identical to the fractional accessibility found for the long-lifetime species in rod monomers (Chang & Ludescher, 1993), indicating that the solvent exposure of the tryptophans in the two aggregation states of the rod is nearly identical.

Time-Resolved Anisotropy. Time-resolved anisotropy decays of tryptophan in rod monomers and rod filaments, calculated directly from the polarized vertical and horizontal emission decay transients, are plotted in Figure 8. The instrument response functions for these decays, also plotted in Figure 8, had a full width at half-maximum of 25 ps; the response function was thus sufficiently fast that only the initial data points of the decays (those overlapping the region of the instrument response function) contained convolution artifacts

Table 2: Fit Parameters from Analysis of the Anisotropy Decay of Myosin Rod Monomers and Filaments[a]

sample[b]	n[c]	r_1	ϕ_1 (ns)	r_2	ϕ_2 (ns)	r_∞	$\chi^2 \times 10^{-4}$
monomer	1	0.070 ± 0.006[d]	2.3 ± 0.5			0.157 ± 0.008	2.16
	2	0.065 ± 0.010	0.64 ± 0.23	0.036 ± 0.004	7.4 ± 2.5	0.151 ± 0.004	1.16
filament	1	0.072 ± 0.005	2.2 ± 0.2			0.153 ± 0.008	2.42
	2	0.076 ± 0.024	0.20 ± 0.07	0.048 ± 0.007	5.7 ± 1.0	0.146 ± 0.006	1.96

[a] Measurements at 20 °C; excitation at 300 nm, emission at 360 nm. [b] Myosin rod monomers in MB and myosin rod filaments in low-salt MB. [c] Data were fit to eq 6 (Materials and Methods); n is the number of exponentials used in the analysis of the anisotropy decay. [d] Standard deviations of the fit parameters calculated from the average of three or more analyses.

(Papenhuijzen & Visser, 1983). A direct analysis of the calculated anisotropy decay thus provided an acceptable method to estimate the anisotropy decay components. The decay curves for tryptophan in rod monomers and filaments were similar, and both decays appeared complex, containing a fast subnanosecond decay followed by a slow nanosecond decay (Figure 8).

The anisotropy decay curves were analyzed directly as a sum of one or two exponentials plus a constant (eq 6 under Materials and Methods); attempts to directly fit the parallel and perpendicular decay transients using deconvolution techniques were unsuccessful for reasons outlined under Materials and Methods. The smooth curves through the data points in Figure 8 represent the best single- or double-exponential fits to the undeconvoluted data. The fit parameters from these analyses (Table 2) were the same within experimental error for monomers or filaments using either single- or double-exponential decays to a constant. This indicates that the rotational dynamics of the tryptophan side chains in either aggregation state of the protein were essentially identical in both amplitude and correlation time.

The decays of either monomers or filaments were better fit by double- that single-exponential decays; the calculated single-exponential decays deviated from the data at both early and intermediate times (Figure 8) and had higher χ^2 values (Table 2). The two-component fits indicated that the tryptophan side chains undergo at least two distinguishable modes of rotational motion: a fast motional mode with a subnanosecond correlation time and a slower motional mode with a 6–7-ns correlation time; each of these motional modes was restricted in amplitude on the time scale of the tryptophan fluorescence.

Although the method of data analysis precluded any detailed analysis of the fast anisotropy decay, the time scale and amplitude of the fast decay were suggestive of fast wobble of the tryptophans on the surface of the α-helical coiled-coil; similar correlation times and amplitudes have been seen in other studies of tryptophan dynamics in proteins (Munro, 1979; Ludescher et al., 1988b). This motion was restricted in amplitude in both monomers and filaments and appeared to have a smaller amplitude in monomers (r_1 = 0.065) than in filaments (r_1 = 0.076), indicating that aggregation to filaments did not restrict, and may have enhanced, the motion of the individual tryptophan side chains.

The long correlation time seen in the anisotropy decay of both monomers and filaments, although better determined in this data analysis, was correspondingly harder to assign to a particular physical mode of motion. The magnitude of the correlation time, identical within error for monomers and filaments, was consistent with the diffusive motion of a larger portion of the coiled-coil region of myosin. The size of the rotating unit can be crudely estimated by calculating the molecular mass of a globular protein with a correlation time in the range 5.7–7.5 ns. This is equivalent to a molecular mass in the range 13–17 kDa; a segment of the coiled-coil of this molecular mass would be about 90–120 Å long. Although an asymmetric cylinder such as myosin rod can rotate faster about its long axis than an equivalent sphere (Cantor & Shimmel, 1980), it is unlikely that the slow motion corresponds to rotational motion about the long axis of the coiled-coil for two reasons. First, the correlation time for rotation about the long axis of monomeric myosin would be about 50 ns (see Materials and Methods), much slower than the observed motions. Second, such a motion could not occur in the aggregated state.

The observed correlation time must therefore reflect internal, segmental motions within the coiled-coil structure similar to those seen in the tropomyosin crystal (Phillips et al., 1980, 1986; Boylan & Phillips, 1986). One possibility is torsional twisting of the two helixes about the long axis of the coiled-coil; such a motion would involve a local change in the pitch of the coiled-coil. Another possibility is a local, internal "breathing" mode in which the two helical chains transiently separate from each other; such a separation could involve a localized relaxation of the helical structure of the individual polypeptide chains (Phillips et al., 1979). These two motions may actually occur together in a concerted change in the local coiled-coil structure. It is unlikely, however, that the motion reflects global unwinding, or fraying, of the coiled-coil structure brought on by removal of the myosin heads. In order to influence the motion of the tryptophans, which are located nearly in the middle of the rod (see Figure 1), such unwinding would have to involve about half of the molecule. Electron microscopic studies of myosin fragments provide no indication for such large-scale unwinding of the coiled-coil (Stewart & Edwards, 1984). Irrespective of the physical interpretation of the observed motion, however, it is clear that there were no detectable changes in the tryptophan motions upon polymerization into filaments. This indicates that aggregation did not significantly change the physical environment of that portion of the rod containing the tryptophans.

CONCLUSION

Filaments formed from myosin rod provide a facile model system that has been used to specifically monitor the S2 region of the crossbridge in myosin filaments (Reisler & Liu, 1982; Ueno et al., 1983; Reisler et al., 1983) and minifilaments (Applegate & Reisler, 1983). These studies of chemical cross-linking and proteolysis indicate that the truncated crossbridges in rod filaments undergo cation-controlled conformational transitions that closely resemble the transitions of the entire crossbridge of myosin filaments.

Our fluorescence results indicate that the tryptophan-containing region of rod filaments was actually in a conformation only subtly different from that found in monomeric myosin. Extensive quantitative similarities in fluorescence properties demonstrated that the local environment, solvent exposure, and rotational dynamics of the myosin rod around these tryptophan residues were essentially unaffected by aggregation of the rod into filaments. This is a surprising

result. Models for the thick filament structure (Huxley, 1963; Pepe, 1966, 1967; Squire, 1973) propose that the body of the thick filament consists of a bundle of LMM segments while the crossbridge consists of short S2 plus some or all of the hinge region (Figure 1). The two pairs of tryptophans in the rod are located within that portion of LMM thought to aggregate into the body of the thick filament (Huxley, 1963; Pepe, 1967; Squire, 1973).

There are two possible interpretations of our fluorescence results. One is that the N-terminal region of LMM containing the tryptophan residues is not actually part of the bundle of coiled-coils in the body of the thick filament but instead forms part of the crossbridge that extends away from the filament surface. The other is that this N-terminal region of LMM is part of the bundle of coiled-coils in the thick filament but that aggregation does not change the local environment of the two pairs of tryptophans.

If the tryptophan-containing region of LMM is not aggregated into the body of the thick filament, then the myosin crossbridge includes more of the rod than previous models suggest. The crossbridge is thought to consist of short S2 and some or all of the hinge region (see Figure 1) delimited by two arginine residues located 430 and 660 Å from the head/rod junction (Sutoh et al., 1978; Lu & Wong, 1985). The two pairs of tryptophans are located in LMM about 820 and 925 Å from the S1/rod junction (Maeda et al., 1987), assuming a rise per residue of 1.5 Å in an α-helix. If these tryptophans are actually part of the crossbridge, then the coiled-coil region of the crossbridge must be nearly 300 Å longer than previous models indicate (that is, be at least 925 Å rather than 660 Å long). Since the entire rod is about 1650 Å long (Lowey & Cohen, 1962), the crossbridge would then comprise over 50% of the length of the myosin rod. If this is true, it is a novel finding and suggests that the hinge region may not play the pivotal role that previous models suggest.

If the tryptophan-containing region of LMM is aggregated into the body of the thick filament, then the thick filament must be organized in such a manner that the tryptophan residues are unperturbed by packing interactions with other subunits. Current models for the packing of coiled-coils in vertebrate muscle thick filaments suggest that the filament is composed of nine subfilaments arranged parallel to the filament axis (Pepe et al., 1986; Ashton et al., 1992). Six of these subfilaments appear to be on the filament surface while the remaining three are located in the filament core (Pepe et al., 1986); this packing scheme may vary along the filament, however, leading to some regions in which all of the subfilaments are located on the filament surface (Ashton et al., 1992) in patterns similar to those seen in insect flight muscle (Beinbrech et al., 1988, 1990). Our fluorescence data are not easily reconcilable with a packing scheme in which three of nine subfilaments form the filament core since such a scheme would bury one-third of the tryptophans, and thus decrease their solvent accessibility. An orientation in which the tryptophan-containing region was located on the filament surface could result in minimal perturbation of the tryptophan environments. Even this packing orientation, however, would appear to require that the molecular interactions between coiled-coils at the surface were sufficiently minor that the solvent accessibility and rotational dynamics of the tryptophans were essentially unaffected by the contacts. Such a packing scheme resembles that expected within a crossbridge.

It is worth noting that our filament experiments were performed at pH 7.0 under conditions in which thick filament crossbridges are thought to be in a compact conformation (Persechini & Rowe, 1984) characterized by low rates of proteolysis and high rates of cross-linking (Reisler & Liu, 1982; Ueno et al., 1983; Applegate & Reisler, 1983; Reisler et al., 1983). In this conformation, the S2 region of the crossbridge may be closely associated with the body of the thick filament (Persechini & Rowe, 1984). Our interpretations thus reflect the structure of what is thought to be the more compact, and thus less extended, conformation of the crossbridge.

A model of a longer crossbridge without a distinct flexible hinge connecting the coiled-coil to the thick filament would force us to rethink the relationship between structure and dynamics in the myosin crossbridge. If the hinge region does not delimit the connection between the crossbridge and the filament, then models of crossbridge dynamics that involve the localized rotation of rigid segments at specific sites may be inappropriate. An alternate possibility, suggested by studies of the high-frequency viscoelastic behavior of myosin (Rosser et al., 1978), myosin rod (Hvidt et al., 1982), and LMM (Hvidt et al. 1983), proposes that the coiled-coil region of myosin (and other fibrous proteins such as tropomyosin) is a continuous, semirigid rod that can undergo bending and flexure uniformaly along its length. A continuously flexible crossbridge with the rigidity of myosin rod can undergo thermally generated fluctuations that would move the head region a significant distance away from the thick filament surface (Hvidt et al., 1982); the extent of these excursions away from the surface increases with the length of the crossbridge.

This study provides tantalizing evidence of the complex character of the rotational dynamics of the coiled-coil crossbridge. There is now direct evidence for rotational correlation times in solution ranging from ≈6 ns (this study) to ≈25 μs (Ludescher et al., 1988a; Ludescher & Thomas, 1988) for the coiled-coil structure that forms the crossbridge; the longer correlation time (≈170 μs) seen *in situ* in relaxed glycerinated muscle fibers (Stein et al., 1990) may also reflect the same physical phenomenon. The continuous flexibility model (Hvidt et al., 1982) easily explains such dynamic complexity in terms of a hierarchy of normal modes of flexural motion of a semirigid rod (Ookobo et al., 1976; Ferry, 1980; Hvidt et al., 1982). Whether such dynamic complexity plays a functional role in coupling the force generated within the actin-bound myosin head to the relative sliding motion of the thick and thin filaments remains moot.

The biological implications of our findings are necessarily limited by the model system that we have used. In order to specifically observe the local conformation of the tryptophan-containing region of LMM in the filament, it was necessary to remove S1 and its associated tryptophans. Although the studies cited above demonstrate that rod filaments have many properties similar to those of myosin filaments, it is possible that, on the local, molecular level, the structure of synthetic rod filaments differs significantly from that of myosin filaments. Native myosin filaments also contain ancillary proteins such as titin, C protein, and H protein which affect the structure of the filament (Sheterline, 1983); even LC2, which binds to the myosin head, appears to modulate the structure of synthetic myosin filaments (Chowrashi et al., 1989). These proteins play important roles in dictating the global structure of native thick filaments within the sarcomere, and such effects may originate in local changes in the packing of coiled-coils within the thick filament. If so, our results may need to be modified in light of future studies of the direct influence of these myosin binding proteins on the structure of the filament.

ACKNOWLEDGMENT

We are particularly grateful to Dr. Scott Williams of the Regional Laser and Biotechnology Lab for expert help in the data analysis.

REFERENCES

Applegate, D., & Reisler, E. (1983) *J. Mol. Biol. 169*, 455.
Ashton, F. T., Weisel, J., & Pepe, F. A. (1992) *Biophys. J. 61*, 1513.
Bagshaw, C. (1982) *Muscle Contraction*, Chapman & Hall, London and New York.
Barkely, M. D., Kowalczyk, A. A., & Brand, L. (1981) *J. Chem. Phys. 75*, 3581.
Beechem, J. M., & Gratton, E. (1988) *Proc. SPIE—Int. Soc. Opt. Eng. 909*, 70.
Beechem, J. M., Gratton, E., Ameloot, M., Knutson, J. R., & Brand, L. (1991) in *Topics in Fluorescence Spectroscopy* (Lakowicz, J. R., Ed.) Vol. 2, pp 241–306, Plenum Press, New York.
Beinbrech, G., Ashton, F. T., & Pepe, F. A. (1988) *J. Mol. Biol. 201*, 557.
Beinbrech, G., Ashton, F. T., & Pepe, F. A. (1990) *Tissue Cell 22*, 803.
Belford, G. G., Belford, R. I., & Weber, G. (1972) *Proc. Natl. Acad. Sci. U.S.A. 69*, 1392.
Boylan, B., & Phillips, G. N. (1986) *Biophys. J. 49*, 76.
Cantor, C. R., & Schimmel, P. R. (1980) *Biophysical Chemistry, Part II: Techniques for the Study of Biological Structure and Function*, W. H. Freeman & Co., San Francisco.
Chang, Y. (1993) Ph.D. Dissertation, Rutgers, The State University, New Brunswick, NJ.
Chang, Y., & Ludescher, R. D. (1992) *Proc. SPIE—Int. Soc. Opt. Eng. 1640*, 159.
Chang, Y., & Ludescher, R. D. (1993) *Biophys. Chem. 48*, 49.
Chang, Y., & Ludescher, R. D. (1994) *Biophys. Chem.* (in press).
Chowrashi, P. K., Pemrick, S. M., & Pepe, F. A. (1989) *Biochim. Biophys. Acta 990*, 216.
Cooke, R. (1986) *CRC Crit. Rev. Biochem. 21*, 53.
Demchenko, A. P. (1986) *Ultraviolet Spectroscopy of Proteins*, Springer-Verlag, Berlin.
Eads, T. M., Thomas, D. D., & Austin, R. H. (1984) *J. Mol. Biol. 178*, 55.
Eftink, M. R. (1991) in *Topics in Fluorescence Spectroscopy* (Lakowicz, J. R., Ed.) Vol. 2, pp 53–126, Plenum Press, New York.
Eftink, M. R., & Ghiron, C. A. (1976) *J. Phys. Chem. 80*, 486.
Eisenberg, E., & Hill, T. L. (1985) *Science 227*, 999.
Ferry, J. D. (1980) *Viscoelastic Properties of Polymers*, 3rd ed., John Wiley & Sons, New York.
Harrington, W. F., & Burke, M. (1972) *Biochemistry 11*, 1448.
Harrington, W. F., & Rodgers, M. E. (1984) *Annu. Rev. Biochem. 53*, 35.
Harvey, S. C., & Cheung, H. C. (1982) in *Cell and Muscle Motility* (Dowben, R. M., & Shay, J. W., Eds.) Vol. 2, pp 279–302, Plenum Press, New York.
Huxley, A. F., & Niedergerke, R. (1954) *Nature 173*, 971.
Huxley, H. E. (1963) *J. Mol. Biol. 7*, 281.
Huxley, H. E. (1969) *Science 164*, 1356.
Huxley, H. E., & Hanson, J. (1954) *Nature 173*, 973.
Huxley, H. E., & Brown, W. (1967) *J. Mol. Biol. 30*, 383.
Hvidt, S., Nestler, F. H. M., Greaser, M. L., & Ferry, J. D. (1982) *Biochemistry 21*, 4064.
Hvidt, S., Ferry, J. D., Roelke, D. L., & Greaser, M. L. (1983) *Macromolecules 16*, 740.
Johnson, D. A., & Yguerabide, J. (1985) *Biophys. J. 48*, 949.
Katsura, I., & Noda, H. (1973a) *J. Biochem. (Tokyo) 73*, 245.
Katsura, I., & Noda, H. (1973b) *Adv. Biophys. 5*, 177.
King, L., & Lehrer, S. S. (1989) *Biochemistry 28*, 3498.
Kodama, T. (1984) *Physiol. Rev. 65*, 467.
Lehrer, S. S. (1971) *Biochemistry 10*, 3254.
Lowey, S., & Cohen, C. (1962) *J. Mol. Biol. 4*, 293.
Lowey, S., Slayter, H. S., Weeds, A. G., & Baker, H. (1969) *J. Mol. Biol. 42*, 1.
Lu, R. C., & Wong, A. (1985) *J. Biol. Chem. 260*, 3456.
Ludescher, R. D., & Thomas, D. D. (1988) *Biochemistry 27*, 3343.
Ludescher, R. D., Eads, T. M., & Thomas, D. D. (1988a) *J. Mol. Biol. 200*, 89.
Ludescher, R. D., Johnson, I. D., Volwerk, J. J., de Haas, G. H., Jost, P. C., & Hudson, B. S. (1988b) *Biochemistry 27*, 6618.
Maeda, K., Sczakiel, G., & Wittinghofer, A. (1987) *Eur. J. Biochem. 167*, 97.
Margossian, S. S., & Lowey, S. (1982) *Methods Enzymol. 85B*, 55.
McLachlan, A. D., & Karn, J. (1982) *Nature 299*, 226.
Munro, I., Pecht, I., & Stryer, L. (1979) *Proc. Natl. Acad. Sci. U.S.A. 76*, 56.
Noyes, R. M. (1961) *Prog. React. Kinet. 1*, 129.
Ookubo, N., Komatsubara, M., Nakajima, H., & Wada, Y. (1976) *Biopolymers 15*, 929.
Papenhuijzen, J., & Visser, A. J. W. G. (1983) *Biophys. Chem. 17*, 57.
Pepe, F. A. (1966) *Electron Microsc. 2*, 53.
Pepe, F. A. (1967) *J. Mol. Biol. 27*, 203.
Pepe, F. A. (1982) in *Cell and Muscle Motility* (Dowben, R. M., & Shay, J. W., Eds.) Vol. 2, pp 141–171, Plenum, New York.
Pepe, F. A. (1983) in *Muscle and Non-muscle Motility* (Stracker, A., Ed.) Vol. 1, pp 105–149, Academic Press, New York.
Pepe, F. A., Ashton, F. T., Street, C., & Weisel, J. (1986) *Tissue Cell 18*, 499.
Persechini, A., & Rowe, A. J. (1984) *J. Mol. Biol. 172*, 23.
Phillips, G. N., Lattman, E. S., Cummins, P., Lee, K. Y., & Cohen, C. (1979) *Nature 278*, 413.
Phillips, G. N., Fillers, J. P., & Cohen, C. (1980) *Biophys. J. 32*, 485.
Phillips, G. N., Fillers, J. P., & Cohen, C. (1986) *J. Mol. Biol. 92*, 111.
Rayment, I., Rypniewski, W. R., Schmidt-Base, K., Smith, R., Tomchick, D. R., Benning, M. M., Winkelmann, D. A., Wesenberg, G., & Holden, H. M. (1993) *Science 261*, 50.
Reisler, E., & Liu, J. (1982) *J. Mol. Biol. 157*, 659.
Reisler, E., Liu, J., & Cheung, P. (1983) *Biochemistry 22*, 4954.
Rosser, R. W., Nestler, F. H. M., Schrag, J. L., Ferry, J. D., & Greaser, M. (1978) *Macromolecules 11*, 1239.
Sheterline, P. (1983) *Mechanisms of Cell Motility: Molecular Aspects of Motility*, Academic Press, London.
Squire, J. M. (1973) *J. Mol. Biol. 77*, 291.
Stein, R. A., Ludescher, R. D., Dahlberg, P. S., Fajer, P. G., Bennett, R. L. H., & Thomas, D. D. (1990) *Biochemistry 29*, 10023.
Steiner, R. F. (1991) in *Topics in Fluorescence Spectroscopy* (Lakowicz, J. R., Ed.) Vol. 2, pp 1–51, Plenum Press, New York.
Stewart, M., & Edwards, P. (1984) *FEBS Lett. 118*, 75.
Sutoh, K., Sutoh, K., Karr, T., & Harrington, W. F. (1978) *J. Mol. Biol. 126*, 1.
Szabo, A. G., & Rayner, D. M. (1980) *J. Am. Chem. Soc. 102*, 554.
Thomas, D. D., Ishiwata, S., Seidel, J. C., & Gergely, J. (1980) *Biophys. J. 32*, 873.
Tregear, R. T., & Marston, S. B. (1979) *Annu. Rev. Physiol. 41*, 723.
Ueno, H., Rodgers, M. E., & Harrington, W. F. (1983) *J. Mol. Biol. 168*, 207.
Warrick, H. M., & Spudich, J. A. (1987) *Annu. Rev. Cell Biol. 3*, 379.
Weeds, A. G., & Taylor, R. S. (1975) *Nature 257*, 54.